RSC Advances

ROYAL SOCIETY OF CHEMISTRY

www.rsc.org/advances

High stability and superior catalytic reactivity of nitrogen−doped graphene supporting Pt nanoparticles as a catalyst for oxygen reduction reaction: a density functional theory study

Yu Tian,[1] Yue−jie Liu,[1] Jing−xiang Zhao,[1,*] Yi−hong Ding[2,*]

[1] *Key Laboratory of Photonic and Electronic Bandgap Materials, Ministry of Education, Harbin Normal University, Harbin, 150025, China*

[2] *State Key Laboratory of Theoretical and Computational Chemistry, Institute of Theoretical Chemistry, Jilin University, Changchun 130023, China*

Abstract: We investigated the structural and electronic properties of Pt_{13} nanoparticles on various nitrogen(N)−doped graphene and their interaction with O by density functional theory (DFT) calculations. The results revealed that the N−doping can greatly enhance the binding strength of Pt_{13} nanoparticles on graphene surface, thus ensuring their high stability. For N_C doping (N atoms directly substituting for C atoms), the enhanced binding strength of Pt_{13} cluster is attributed to the activation of the carbon atoms around N−dopant, while the strong hybridization of the *d* states of Pt_{13} cluster with the sp^2 dangling bonds of the N atoms in defective N−doped graphenes contributes to the strong adsorption. Moreover, a certain amount of electrons are transferred from Pt_{13} to substrate accompanied by a substantial downshift of Pt_{13} *d*−band center, thus greatly weakening the interaction of O on these composites: the adsorption energy of O is reduced from −3.70 eV on freestanding Pt_{13} nanoparticle to −1.762, −1.723, and −1.507 eV on deposited Pt_{13} ones on N_C, 3NV, and 4ND structures, respectively. Hence, it is expected that N−doped graphene

supported Pt nanoparticles exhibit super catalytic reactivity in ORR.

1. Introduction

Two−dimensional material graphene, one planar sheet of sp^2−bonded carbon atoms arranged in a hexagonal lattice, is attractive to a wide variety of research fields due to its unique optical, electrical, magnetic, and mechanical properties.[1-3] The metal/graphene heterostructures provide unique properties for many applications such as biosensors, nanodevices, and heterogeneous catalysis.[4-9] Due to the large surface area, outstanding electronic and thermal conductivity, as well as the high mechanical strength and potential low production cost, graphene has been regarded as an excellent support material for dispersion of metal nanoparticle catalysts.[2,3] Besides, metal/graphenes are shown to be used as catalysis in fuel cells fileds.[10] Achieving a favorable balance between the good stability and high catalytic activity of metal/graphene systems is vital to evaluate their potentials for the development of fuel cells.

Unfortunately, the pristine graphene is relatively inert, leading to its weak interaction with the metal clusters. Thus, the adsorbed metal clusters can diffuse fairly easily along the surface of graphene,[11] resulting in eventual catalyst sintering. In this sense, despite its unique properties such as excellent electrical conductivity and structural stability, the pristine graphene is not a suitable support unless appropriate strategies are proposed to trap and immobilize metal clusters.[12] Chemical doping with a secondary (noncarbon) element has been shown to be effective in modifying the

intrinsic properties of graphene, including electronic and magnetic characteristics.[13] More importantly, doping might endow graphene with high chemical reactivity,[14] which greatly broadens their applications.

Among various possible dopants (such as B,[15,16] N,[17] S,[18] F,[19] and P[20]), N−doping exhibits obvious advantages: (1) a facile doping process and effective modulation of graphitic structures, electronic, and magnetic properties;[21-26] (2) N with excessive valence electrons may provide additional *p*−electrons in a graphitic plane.[27,28] These properties make N−doped graphene have many attractive applications, such as flexible electronics, energy conversion/storage devices, and catalysts.[29] In particular, N−doped graphene has been shown to be a superior support for the dispersion of metal clusters.[30-34] In comparison to conventional supports, laboratory studies have pointed out that the N−doping increases the efficiency of the proton−exchange membrane fuel cells, as it increases the dispersion of the metal catalyst,[35] prevents metal agglomeration,[36] and participates in the oxygen reduction reaction (ORR) as active sites for catalysis.[32, 37,38]

Compared with the above experimental advances, we note that the theoretical studies on the deposit of metal nanoparticles on N−doped graphene are very lack (only a single metal atom has been previously considered),[39,40] especially on the potential applications of the metal/N−doped graphene composites in ORR. Hence, in the present work, we have studied the adsorption of Pt nanoparticles, which represent one of the best electrocatalysts for ORR, on three kinds of N−doped graphene, including graphitic N (N atoms directly substituting for C atoms, labeled as N_C),

pyridinic N (N atoms substituting for C atoms around a monovacancy, labeled as 3NV), and porphyrinic N (N atoms substituting for C atoms around a divacancy, labeled as 4DV). The following key questions would be addressed: (1) the stability of Pt nanoparticles on the three kinds of N−doped graphenes, (2) the electronic properties of these composites, and (3) their catalytic performance in ORR.

2. Computational details

Calculations were based on the spin−polarized DFT using the generalized gradient approximation (GGA) for the exchange−correlation potential prescribed by Perdew−Burke−Ernzerhof (PBE),[41] which was implemented in DMol^3 package.[42, 43] All−electron calculations were employed with the double numerical basis sets plus polarization functional (DNP), which are comparable to the Gaussian 6−31G (d,p) basis set in size and quality. A (5 × 5) supercell with the periodic boundary conditions on the $x-y$ plane was employed according to the test for the effects of the size of supercell on the adsorption energy as shown in Table S1 of **Supporting Information**. In the current study, Pt_{13} clusters have been chosen to investigate the interaction of a Pt nanoparticle on N−doped graphene because they match the first magic number[44,45] according to the geometric shell closing model and have a higher geometric and electronic stability than other cluster sizes. The vacuum space was set with 30 Å in the z direction to avoid the interactions between periodic images. In accordance with a preliminary test (see Table S1), the Brillouin zone of the super cell was sampled by 2 × 2 × 1 points with the Monkhrost-Pack scheme[46] during the geometric optimization.

All structures were fully relaxed without any symmetry constraints. Convergence in energy, force, and displacement were set as 10^{-5} Ha, 0.002 Ha/ Å, and 0.005 Å, respectively. The Hirshfeld method[47] was adopted to calculate the charge transfer.

The binding energy (E_b) of a Pt_{13} cluster on the N−doped graphene was defined as $E_b = E_{Pt_{13}/substrate} - (E_{substrate} + E_{Pt_{13}})$, where $E_{Pt_{13}/substrate}$, $E_{substrate}$, and $E_{Pt_{13}}$ stand for the total energy of Pt_{13}/substrate, N−doped graphene, and the freestanding Pt_{13} cluster, respectively. Moreover, for the study on O adsorption, the adsorption energy (E_{ads}) relative to $1/2O_2$ (g) was defined as $E_{ads} = E_{total}(O_{ads}-Pt_{13}/substrate) - E_{total}(Pt_{13}/substrate - E_{total}(O_2)/2$, where E_{total} is the total energies of the systems in parentheses.

3. Results and Discussion

3.1. The Binding of Pt_{13} Cluster on N–doped Graphenes. In Figure 1, we list the geometric structures and electronic properties of the three N−doped graphenes. It is found that graphene still remains planar structure in the three doped structures. The average C−N bond lengths are 1.443 (for N_C), 1.352 (for 3NV), and 1.354 Å (for 4DV), respectively. Moreover, the calculated formation energies of the three N−doped graphenes are 1.059 (for N_C), 3.577 (for 3NV), and 4.321 eV (for 4DV), respectively, suggesting that the graphitic N is easier to be formed than other two N−doping structures. Note that the formation energy was calculated according to the following definition: $E_{formation} = E_{total} - n_C\mu_C - n_N\mu_N$, where E_{total} is the total energy of the N−doped graphenes, nanotube, n_C and n_N are the number of C and N atoms,

respectively, and μ is the chemical potential. μ_C was calculated from C in the corresponding pristine graphene, while μ_N was obtained from N in the gas phase (N_2 molecule). The DOS curves of N_C, 3NV, and 4ND are shown in Figure 1. Due to the higher DOS intensity near Fermi level, 3NV and 4ND structures are expected to be more activity as compared with N_C one. Hence, the defective N−doped graphenes might provide more reactive anchoring points to stabilize the deposited Pt nanoparticles.

In light of the extremely expensive cost for searching for the stable configuration of a Pt_{13} cluster with various shapes on these N−doped graphenes, the Pt_{13} cluster with the distorted cuboctahedron configuration with D_{4h} symmetry was employed in this work, since it is more stable than the other symmetry[48-50] and has been successfully used in previous studies.[49-52] The Pt_{13} clusters were introduced at different configurations orientations with respect to the sheet (e.g., with a triangular or square face parallel to the sheet, a vertex closest to the sheet, and so on). After geometrical optimizations for each initial configuration, the obtained lowest−energy structures are displayed in Figure 2; the corresponding binding energies, charge transfer, and structural parameters are given in Table 1.

As seen from these data, a Pt_{13} cluster can most favorably adsorb on the N_C structure via one of the triangular faces, in which each Pt atom is attached to the C−C bond near the N−site (Figure 2a), instead of binding directly to the N atom. This happens because the nitrogen atom in the graphene structure uses three valence electrons to form σ bands, one valence electron to form a π bond, and places the

remaining electron in the higher energy π* state, leading to such ‘‘donor−like’’ behavior in this N−doped graphene, which is similar to the case of N−doped carbon nanotube.[53] The shortest distance of the newly formed Pt−C bond (i.e. Pt9−C1 in Figure 2a) is about 2.153 Å. On 3NV structure, Pt_{13} uses one vertex Pt atom to saturate the three dangling N atoms around defects, forming a near substitutional configuration with the shortest Pt−N bond (i.e. Pt7−N in Figure 2b) of 2.105 Å. Meanwhile, one other Pt atom interacts with the basal C−C bond and the shortest distance of the Pt−C bond (i.e. Pt8−C2 in Figure 2b) is 2.166 Å. Upon Pt_{13} adsorption on 4ND configuration, one apex atom is bound with the four N atoms at the divacancy site, forming a cross configuration. The shortest Pt−N bond length (i.e. Pt13−N in Figure 2c) is 2.011 Å. Meanwhile, two other Pt atoms (Pt10 and Pt12) bind with the C atoms of graphene.

Another important result in Table 1 is that the Pt_{13} cluster can be stably adsorbed on the three N−doped graphenes. The calculated binding energies of the Pt_{13} cluster are −4.451 (for N_C), −6.495 (for 3NV), and −8.331 eV (for 4ND), respectively. For comparison, we also calculated the adsorption of the Pt nanoparticle on the perfect graphene. The results indicate that the Pt_{13} nanoparticle has an adsorption energy of −0.250 eV on pristine graphene, which is slightly smaller than that of previous study (−0.360 eV) due to the difference in the employed methods.[54] Obviously, the pristine graphene sheet is unstable for anchoring of a Pt nanoparticle because effective bonding is absent. Relative to a pristine graphene sheet, the existence of 3NV and 4ND structures in graphene greatly enhances the adsorption capability of a Pt_{13} cluster.

Although the N−doping in the three substrates can assist the adsorption of the Pt_{13}cluster on graphene, the detailed mechanisms are very different. For a N_C structure, the enhanced adsorption comes from the activation of the N−neighboring C atoms as shown above. By contrast, the enhancement in Pt_{13} cluster on 3NV or 4ND is attributed to the strong hybridization between the *d* orbitals of Pt_{13} cluster and the sp^2 dangling bonds of the neighboring N atoms near the vacancy. Due to the significantly strong binding strength of Pt_{13} cluster on these N-doped graphene, it can be expected that the structures of adsorbates and substrates are distorted in various ways. For example, the distances of the N−N bonds in 3NV and 4DV structures are elongated by 0.238 and 0.258 Å, respectively, while the average Pt−Pt bond length is elongated by ~0.120 Å. This is in good agreement with previous studies: a stronger adsorption would lead to a greater distortion in adsorbate-substrate system.[49, 55] Considering the large binding energy of Pt nanoparticle on these N-doped graphene, the deposited Pt nanoparticle exhibit high stability by preventing its sintering.

In addition, taking 3NV structure as an example, we also considered the deposition of several meta−stable Pt_{13} nanoparticles including C_{4v}, D_{5h}, O_h, and I_h symmetry structures. The obtained most−stable configurations of Pt_{13} nanoparticles with C_{4v}, D_{5h}, O_h, and I_h symmetry structures on the three N−doped graphenes are presented in Figure S1. We found that these meta−stable Pt_{13} clusters can also stably be adsorbed on substrates. The calculated binding energies of these meta-stable Pt_{13} clusters on the three N−doped graphenes are smaller than those of the most stable configurations in Figure 2. We should point out that the lowest energy structure for

Pt_{13} cluster was recently reported, in which the average Pt−Pt bond length is about 2.620 Å.[56] Indeed, Pt_{13} cluster tends to adopt more open and low−symmetry morphology. Upon adsorption on 3NV structure in graphene, this configuration (see Figure S1e) is slightly stable by 0.353 eV than that of with D_{4h} symmetry. This suggests that further investigation should first focus on determining at least a few candidate low-energy structures before addressing issues related to the catalytic activity of clusters. Similarly, this deposited Pt_{13} cluster is also distorted due to its strong interaction with substrate.

3.2. Electronic properties of Pt nanoparticles/N−doped graphene composites. After searching for the obtained most stable configurations of Pt_{13}/N−doped graphenes, we further explored the effects of substrates on the electronic properties by analyzing the projected density of states (PDOS), which are useful for deeply understanding the details of the interaction of Pt_{13} nanoparticles with N−doped graphene. Figure 3 shows the plots of the PDOS of the *s*, *p*, and *d* states of Pt atoms and *s* and *p* states of C or N atoms at the support−cluster interface that are involved in bond formation.

It can be seen from PDOSs that a strong hybridization of *d* states of Pt cluster with *p* states of substrates can be obviously observed, especially on 3NV and 4ND structures. This can be expected, because the Pt_{13} cluster uses its valence electrons to saturate the dangling bond of N atoms around the vacancy in the two defective N−doped graphenes. Such interaction results in the large calculated binding energies. Compared with the narrow and sharp bands characterized by a set of discrete levels of

isolated Pt_{13} nanoparticle (Figure S2a), all the Pt states on the three N−doped graphenesare downshifted from the Fermi level and overlap with the *p* states of the substrates and their main peaks are shifted to −1.550 (for N_C), −1.500 (for 3NV), −3.930 eV (for 4ND), respectively. For other Pt atoms far from the interface, their PDOSs are also downshifted from the Fermi level in different ways as shown in Figure S2. The strong binding strength between Pt_{13} nanoparticle and these N−doped graphenes can be further supported by the charge−density difference plots in Figure 3, which show significant redistribution of charge in the vicinity of the support−cluster interface. Note that we calculate the charge−density difference of these fully relaxed configurations as follows: $\Delta\rho = \rho(Pt_{13}/\text{N−doped graphene}) - \rho(\text{N−doped graphene}) - \rho(Pt_{13})$, where $\rho(Pt_{13}/\text{N−doped graphene})$, $\rho(\text{N−doped graphene})$, $\rho(Pt_{13})$ are charge densities of Pt_{13}/N−doped graphene, N−doped graphene, and Pt_{13} cluster, respectively. From Table 1, it is apparent that, regardless of the substrate, the direction of charge transfer is from the Pt_{13} particle to the substrate. The amount of charge transfer to N_C, 3NV, and 4ND structures is 0.165, 0.244, and 0.331 *e*, respectively, according to the Hirshfeld analysis, which is consistent with the order of the binding energy. The above changes in PDOS and charge−density of the interfacial Pt atoms testify that the support of the N−doped graphene has great effects on the electronic structures of the deposited clusters.

3.3. Catalytic activity of Pt nanoparticles/N−doped graphene composites for oxygen reduction reaction (ORR). Recently, the proposed "*d*−band center (ε_d)" by Nørskov and Hammer[57] has been widely used in various transition metal−based

systems. This concept can provide reasonable explanations for the catalytic performance of these catalysts.[51, 58-62] For example, Zhang et al. have suggested that the position of the *d*−band center is the determining factor for the adsorption strength of CO and O_2 on free and defective graphene-supported Au-Pd bimetallic clusters.[63] To evaluate the effects of N−doped graphene support on the catalytic activity of Pt_{13} clusters, we calculated the ε_d of the deposited Pt_{13} clusters on the three N−doped graphenes with respect to the corresponding vacuum level (E_{vac}). For the isolated Pt_{13} cluster, its averaged ε_d is −1.960 eV, in which the ε_d values of the Pt atoms in the center and vertex are −3.940 and −1.790 eV, respectively. As compared to the free counterpart, the Pt nanoparticles on N−doped graphene show significantly changed ε_d as seen in Table 2. For all deposited Pt nanoparticles, the ε_d's are down−shifted from the Fermi level, in agreement with the analysis of PDOS. The average ε_d values of the Pt nanoparticle on N_C, 3NV, and 4ND structures are −2.460, −2.492, and −2.521 eV, respectively. According to the *d*−band model, the lower the averaged ε_d values, the lower reactivity of the deposited Pt particles and the lower possibility for O−poisoning to take place. The above results further suggest the great effect of N−doped graphene on the catalytic reactivity of the supported Pt nanoparticles.

As is known, for the ORR, the adsorption of O_2 molecule on catalyst to form a superoxide together with an electron and proton transfer is the rate−determining step.[64] Thus, a more reactive catalyst, such as Pt nanoparticle (NP) whose d−band center is adjacent to the Fermi level, may bind the O_2 more strongly. This enables the electron transfer and O−O bond breaking to become facile.[57] As a secondary effect,

however, the desorption kinetics of some produced species (namely, O, OH, and OOH) in the subsequent reactions may be slow due to their strong adsorption on catalyst. As a result, the reactive sites of catalyst are occupied by these intermediates, resulting in the sluggish ORR kinetics.[65] Therefore, a good ORR catalyst should be the one that forms a moderate bond with the adsorbates to balance the kinetics of O−O bond breaking and removal of the oxygen−containing species generated from the former step. One method to improve the ORR kinetics of Pt NP composites is to weaken the oxygen adsorption energy by lowering their d−band centers. So, the binding strength of O-containing intermediates is a key indicator to evaluate the catalytic activity trends across different catalysts. It has been found that the adsorption energy of OH and OOH correlate linearly with that of O.[66] In this regard, we focused our investigation of the O adsorption on these supported Pt nanoparticle on N−doped graphene, which can be adopted as an effective indicator of activity to predict activity trends across different catalysts.[58,62]

On freestanding Pt_{13} cluster, it is relatively straightforward to identify via symmetry arguments a minimal set of binding sites (on−top, bridge, hollow sites) for O adsorption studies. Our results indicate that the O prefers to adsorb at a 3−fold site on a surface of the Pt_{13} cluster. The calculated nearest Pt−O distance is 2.100 Å and the adsorption energy is −3.700 eV, while Li et al. reported a larger adsorption energy.[67] The discrepancy in the calculated adsorption energy arises from the fact that the present calculations adopt PBE functional, while RPBE functional was used in Li's work. In fact, our calculated O adsorption energy −4.503 eV on free Pt_{13} cluster

using the RPBE functional is consistent with Li's work.[67] Upon O adsorption on deposited Pt_{13} clusters, similar on−top/bridge/hollow binding sites can also be identified. However, reduced (or complete lack of) symmetry renders each of these sites in deposited Pt_{13} clusters be unique. So we considered many adsorption sites (up to 38) on every cluster. After geometric optimization for each initial O adsorption configuration, the obtained most stable adsorption configurations and the corresponding E_{ads} are presented in Figure 4, while the metastable configurations are summarized in Table S2.

As expected from the *d*−band center analysis, the formation of strong interfacial interaction of Pt_{13} particle with these N−doped graphenes weakens the adsorption of O. The E_{ads} values of O on the deposited one on N_C, 3NV, and 4ND structures are −1.762, −1.723, and −1.507 eV, respectively, which are lower by 1.938, 1.977, and 2.193 eV than that of on isolated Pt_{13} cluster. The low adsorption energies of the Pt_{13}/N−doped graphenes indicate the high activity of these composites in ORR. In other words, Pt nanoparticles deposited on N−doped graphenes not only possess high stability, but also exhibit good catalytic performance in ORR. More importantly, the obtained N-doped graphenes show good catalyst supports for dispersing Pt nanoparticles and the Pt/N−doped graphenes nanomaterials exhibit high electrocatalytic activity toward ORR. As previously reported,[49, 55] the strong adsorption of oxygen on free Pt nanoparticle is attributed to the geometry distortion of the free Pt cluster upon oxygen adsorption. On the contrary, these N-doped graphenes can stably anchor the Pt nanoparticle and thus prevents the Pt_{13} nanoparticle from

being significantly changed upon oxygen adsorption. This may be the reason that O exhibits weaker adsorption on the supported Pt cluster than that of on free one, thus enhancing this system's catalytic performance.

We also note that a vacancy site without N-doping in graphene can also serves as the anchoring point and increase the catalytic activity of Pt nanoparticles by preventing their sintering.[49, 55] For example, the binding energy of Pt_{13} cluster on graphene with monovacancy is -7.120 eV,[49] which is larger than that of on 3NV structure (-6.495 eV). The average ε_d value of the Pt_{13} cluster on defective graphene is about -2.240 eV, which is higher than that of on 3NV structure (-2.492 eV). Thus, the Pt nanoparticle supported by N-doped defective graphene might exhibit higher catalytic performance for ORR.

4. Conclusions

The effects of N−doped graphene support on the electronic properties and catalytic reactivity in oxygen reduction reaction have been studied by density functional theory calculations. The calculated binding energies of Pt_{13} cluster on the three kinds of N−doped graphene are −4.451, −6.495, and −8.331 eV, respectively, suggesting that N−doping greatly enhances the binding strength of Pt_{13} nanoparticle on graphene, although the detailed mechanisms are very different. Dopant nitrogen atom in N_C serves to mediate the enhancement in the adsorption of Pt nanoparticle by activating nitrogen−neighboring carbon atoms. In contrast, the enhanced platinum adsorption in defective N−doped graphene can be mainly attributed to a strong

hybridization between platinum *d* orbitals and sp^2 dangling bonds at the defect sites. In this sense, these N−doped graphene can be used as templates for the Pt clusters assembly, ensuring their stability. The strong interaction induces the shift of the averaged *d*−band center of the deposited Pt nanoparticles from −1.960 eV of the isolated Pt_{13} to the present −2.460 (on N_C structure), −2.492 (on 3NV structure), and −2.521 eV (on 4ND structure), respectively. Thus, it is understandable that O adsorption on Pt_{13}/N−doped graphene is lower than that on freestanding Pt_{13} particle, which is directly correlated with the corresponding shift of their ε_d values. These results indicate that N−doped graphenes not only stabilize the Pt clusters but also enhance their catalytic performance in the oxygen reduction reaction.

Acknowledgment. This work is supported by the National Basic Research Program of China (973 Program, No. 2012CB932800), National Nature Science Foundation of China (No. 21203048) and the Excellent Young Foundation of Harbin Normal University (No. XKYQ201304). The authors would like to show great gratitude to the reviewers for raising invaluable comments and suggestions.

Reference

1. A. K. Geim, *Science*, 2009, 324, 1530-1534.

2. C. N. R. Rao, A. K. Sood, K. S. Subrahmanyam and A. Govindaraj, *Angew. Chem. Int. Ed.*, 2009, 48, 7752-7777.

3. M. J. Allen, V. C. Tung and R. B. Kaner, *Chem. Rev.*, 2010, 110, 132-145.

4. C. Tan, X. Huang and H. Zhang, *Mater. Today*, 2013, 16, 29-36.

5. P. V. Kamat, *J. Phys. Chem. Lett.*, 2011, 2, 242-251.

6. Y. Shao, S. Zhang, C. Wang, Z. Nie, J. Liu, Y. Wang and Y. Lin, *J. Power Sources*, 2010, 195, 4600-4605.

7. G. Fu, Z. Liu, Y. Chen, J. Lin, Y. Tang and T. Lu, *Nano Research*, 2014, 7, 1205-1214.

8. Y. Shao, J. Wang, H. Wu, J. Liu, I. A. Aksay and Y. Lin, *Electroanalysis*, 2010, 22, 1027-1036.

9. X. Li, G. Zhang, X. Bai, X. Sun, X. Wang, E. Wang and H. Dai, *Nat Nanotechnol*, 2008, 3, 538-542.

10. M. Liu, R. Zhang and W. Chen, *Chem. Rev.*, 2014, 114, 5117-5160.

11. Y. Gan, L. Sun and F. Banhart, *Small*, 2008, 4, 587-591.

12. I. Fampiou and A. Ramasubramaniam, *J. Phys. Chem. C*, 2012, 116, 6543-6555.

13. H. Liu, Y. Liu and D. Zhu, *J. Mater. Chem.*, 2011, 21, 3335-3345.

14. X.-K. Kong, C.-L. Chen and Q.-W. Chen, *Chem. Soc. Rev.*, 2014, 43, 2841-2857.

15. O. Stephan, P. M. Ajayan, C. Colliex, P. Redlich, J. M. Lambert, P. Bernier and P. Lefin, *Science*, 1994, 266, 1683-1685.

16. E. A. Ekimov, V. A. Sidorov, E. D. Bauer, N. N. Mel'nik, N. J. Curro, J. D. Thompson and S. M. Stishov, *Nature*, 2004, 428, 542-545.

17. X. Wang, X. Li, L. Zhang, Y. Yoon, P. K. Weber, H. Wang, J. Guo and H. Dai, *Science*, 2009, 324, 768-771.

18. Z. Yang, Z. Yao, G. Li, G. Fang, H. Nie, Z. Liu, X. Zhou, X. a. Chen and S.

Huang, *ACS Nano*, 2011, 6, 205-211.

19. Y. S. Lee, T. H. Cho, B. K. Lee, J. S. Rho, K. H. An and Y. H. Lee, *J. Fluorine Chem.*, 2003, 120, 99-104.

20. Y. Zhang, T. Mori, J. Ye and M. Antonietti, *J. Am. Chem. Soc.*, 2010, 132, 6294-6295.

21. R. Czerw, M. Terrones, J. C. Charlier, X. Blase, B. Foley, R. Kamalakaran, N. Grobert, H. Terrones, D. Tekleab, P. M. Ajayan, W. Blau, M. Rühle and D. L. Carroll, *Nano Lett.*, 2001, 1, 457-460.

22. Y. Xia and R. Mokaya, *Adv. Mater.*, 2004, 16, 1553-1558.

23. D. Wei, Y. Liu, Y. Wang, H. Zhang, L. Huang and G. Yu, *Nano Lett.*, 2009, 9, 1752-1758.

24. W. J. Lee, U. N. Maiti, J. M. Lee, J. Lim, T. H. Han and S. O. Kim, *Chem Comm.*, 2014, 50, 6818-6830.

25. Y. Li, Z. Zhou, P. Shen and Z. Chen, *ACS Nano*, 2009, 3, 1952-1958.

26. Q. Tang, Z. Zhou and Z. Chen, *Nanoscale*, 2013, 5, 4541-4583.

27. S. Latil, S. Roche, D. Mayou and J. C. Charlier, *Phys. Rev. Lett.*, 2004, 92, 256805.

28. K.-Y. Chun, H. S. Lee and C. J. Lee, *Carbon*, 2009, 47, 169-177.

29. H. Wang, T. Maiyalagan and X. Wang, *ACS Catal.*, 2012, 2, 781-794.

30. S. Stambula, N. Gauquelin, M. Bugnet, S. Gorantla, S. Turner, S. Sun, J. Liu, G. Zhang, X. Sun and G. A. Botton, *J. Phys. Chem. C*, 2014, 118, 3890-3900.

31. B. P. Vinayan and S. Ramaprabhu, *Nanoscale*, 2013, 5, 5109-5118.

32. J. Bai, Q. Zhu, Z. Lv, H. Dong, J. Yu and L. Dong, *Int. J. Hydrogen Energy*, 2013, 38, 1413-1418.

33. R. Imran Jafri, N. Rajalakshmi and S. Ramaprabhu, *J. Mater. Chem.*, 2010, 20, 7114-7117.

34. K. Jukk, N. Kongi, L. Matisen, T. Kallio, K. Kontturi and K. Tammeveski, *Electrochim. Acta*, 2014, 137, 206-212.

35. L.-S. Zhang, X.-Q. Liang, W.-G. Song and Z.-Y. Wu, *Phys. Chem. Chem. Phys.*, 2010, 12, 12055-12059.

36. T. Holme, Y. Zhou, R. Pasquarelli and R. O'Hayre, *Phys. Chem. Chem. Phys.*, 2010, 12, 9461-9468.

37. P. Wang, Z. Wang, L. Jia and Z. Xiao, *Phys. Chem. Chem. Phys.*, 2009, 11, 2730-2740.

38. N. Alexeyeva, E. Shulga, V. Kisand, I. Kink and K. Tammeveski, *J. Electroanal. Chem.*, 2010, 648, 169-175.

39. M. N. Groves, C. Malardier-Jugroot and M. Jugroot, *J. Phys. Chem. C*, 2012, 116, 10548-10556.

40. C. L. Muhich, J. Y. Westcott, T. C. Morris, A. W. Weimer and C. B. Musgrave, *J. Phys. Chem. C*, 2013, 117, 10523-10535.

41. J. P. Perdew, K. Burke and M. Ernzerhof, *Phys. Rev. Lett.*, 1996, 77, 3865-3868.

42. B. Delley, *J. Chem. Phys.*, 1990, 92, 508-517.

43. B. Delley, *J. Chem. Phys.*, 2000, 113, 7756-7764.

44. I. A. Solov'yov, A. V. Solov'yov, W. Greiner, A. Koshelev and A. Shutovich, *Phys.*

Rev. Lett., 2003, 90, 053401.

45. F. Baletto and R. Ferrando, *Rev. Mod. Phys.*, 2005, 77, 371-423.

46. H. Monkhorst and J. Pack, *Phys. Rev. B*, 1976, 13, 5188-5192.

47. F. L. Hirshfeld, *Theor. Chim. Acta*, 1977, 44, 129-138.

48. E. Aprà and A. Fortunelli, *J. Phys. Chem. A*, 2003, 107, 2934-2942.

49. D.-H. Lim and J. Wilcox, *J. Phys. Chem. C*, 2011, 115, 22742-22747.

50. D.-H. Lim and J. Wilcox, *J. Phys. Chem. C*, 2012, 116, 3653-3660.

51. D. Xu, Y.-j. Liu, J.-x. Zhao, Q.-h. Cai and X.-z. Wang, *J. Phys. Chem. C*, 2014, 118, 8868-8876.

52. G. Kim and S.-H. Jhi, *ACS Nano*, 2011, 5, 805-810.

53. Y.-H. Li, T.-H. Hung and C.-W. Chen, *Carbon*, 2009, 47, 850-855.

54. S.-Y. Wu and J.-J. Ho, *J. Phys. Chem. C*, 2014, 118, 26764-26771.

55. D.-H. Lim, A. S. Negreira and J. Wilcox, *J. Phys. Chem. C*, 2011, 115, 8961-8970.

56. M. J. Piotrowski, P. Piquini, Z. Zeng and J. L. F. Da Silva, *J. Phys. Chem. C*, 2012, 116, 20540-20549.

57. B. Hammer and J. K. Norskov, in *Adv. in Catal., Vol 45: Impact of Surface Science on Catalysis*, eds. B. C. Gates and H. Knozinger, Elsevier Academic Press Inc, San Diego, 2000, vol. 45, pp. 71-129.

58. X. Liu, L. Li, C. G. Meng and Y. Han, *J. Phys. Chem. C*, 2012, 116, 2710-2719.

59. X. Liu, K. X. Yao, C. G. Meng and Y. Han, *Dalton Trans.*, 2012, 41, 1289-1296.

60. X. Liu, C. G. Meng and Y. Han, *Nanoscale*, 2012, 4, 2288-2295.

61. X. Liu, C. Meng and Y. Han, *Phys. Chem. Chem. Phys.*, 2012, 14, 15036-15045.

62. X. Liu, C. G. Meng and Y. Han, *J. Phys. Chem. C*, 2013, 117, 1350-1357.

63. W. Zhang, D. Cheng and J. Zhu, *RSC Advances*, 2014, 4, 42554-42561.

64. M. Shao, in *Electrocatalysis in Fuel Cells*, ed. M. Shao, Springer London, 2013, vol. 9, ch. 17, pp. 513-531.

65. J. K. Nørskov, J. Rossmeisl, A. Logadottir, L. Lindqvist, J. R. Kitchin, T. Bligaard and H. Jónsson, *J. Phys. Chem. C*, 2004, 108, 17886-17892.

66. F. Abild-Pedersen, J. Greeley, F. Studt, J. Rossmeisl, T. Munter, P. Moses, E. Skúlason, T. Bligaard and J. Nørskov, *Phys. Rev. Lett.*, 2007, 99.

67. L. Li, A. H. Larsen, N. A. Romero, V. A. Morozov, C. Glinsvad, F. Abild-Pedersen, J. Greeley, K. W. Jacobsen and J. K. Nørskov, *J. Phys. Chem. Lett.*, 2012, 4, 222-226.

Table 1. Structural parameters, binding energies, and charge transfer of Pt_{13} particle on various N-doped graphenes.

	E_b (eV)	min d_{Pt-C} (Å)	min d_{Pt-N} (Å)	min/max d_{Pt-Pt} (Å)	Q (e)
N_C	−4.451	2.153	2.987	2.564/4.500	0.165
3NV	−6.495	2.166	2.105	2.594/4.669	0.244
4ND	−8.331	2.181	2.011	2.583/4.462	0.331

Table 2. Change of d-bandcenter (ε_d, eV) before and after Pt_{13} deposition

	isolated Pt_{13}	Pt_{13}/N_C	Pt_{13}/3NV	Pt_{13}/4ND
Pt1	-1.790	-1.860	-2.472	-2.448
Pt2	-1.790	-2.568	-2.273	-2.195
Pt3	-1.790	-2.408	-2.638	-2.579
Pt4	-1.790	-2.469	-2.381	-2.181
Pt5	-1.790	-2.595	-2.136	-1.896
Pt6	-1.790	-1.902	-2.076	-2.640
Pt7	-1.790	-2.656	-4.104	-1.993
Pt8	-1.790	-2.143	-2.653	-2.089
Pt9	-1.790	-2.740	-2.417	-2.450
Pt10	-1.790	-2.762	-2.270	-2.731
Pt11	-1.790	-3.045	-2.866	-2.541
Pt12	-1.790	-2.331	-1.917	-2.352
Pt13	-3.940	-2.496	-2.194	-4.677
average	-1.960	-2.460	-2.492	-2.521

[a] See Figure 2 for the notation of the Pt atoms.

FIGURE CAPTIONS

Figure 1. Optimized structures of N–doped graphenes with (a) N_C, (b) 3NV, and (c) 4ND structures, along with their corresponding projected DOS (C: gray, N: blue. The blue lines correspond to *p*-DOS, and the red lines correspond to *s*-DOS. The green dotted lines correspond to Fermi level.)

Figure 2. Optimized configurations of Pt_{13} particles on N-doped graphenes with (a) N_C, (b) 3NV, and (c) 4ND structures.

Figure 3. DOSs of interfacial C/N and Pt atoms and the corresponding contour plots of differential charge density of Pt_{13} deposition on various N-doped graphenes with (a) N_C, (b) 3NV, and (c) 4ND structures. The Fermi level is set as zero in red dotted lines. The charge accumulation region is rendered in red, and the charge depletion region is in green. The isovalue is ±0.004 au.

Figure 4. The obtained most configurations of O adsorption on deposited Pt_{13} on various N-doped graphenes with (a) N_C, (b) 3NV, and (c) 4ND structures and the corresponding adsorption energies. The unit of bond length is Å.

Figure 1

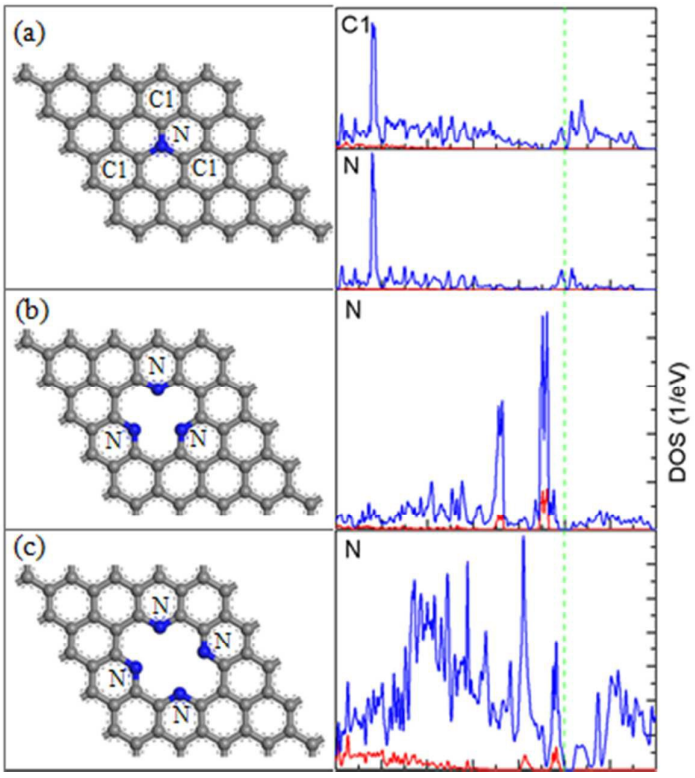

Figure 2

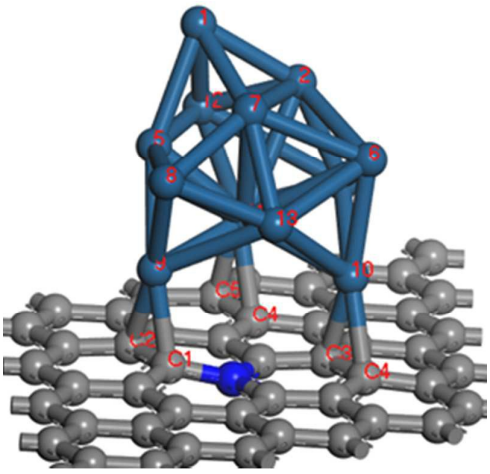

(a)

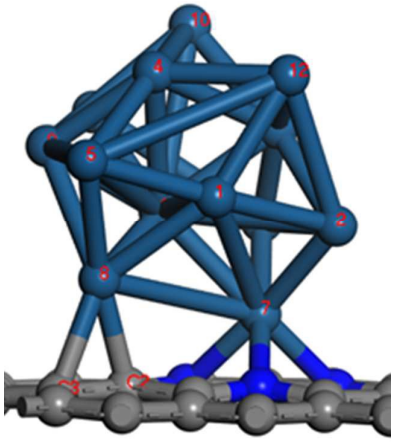

(b)

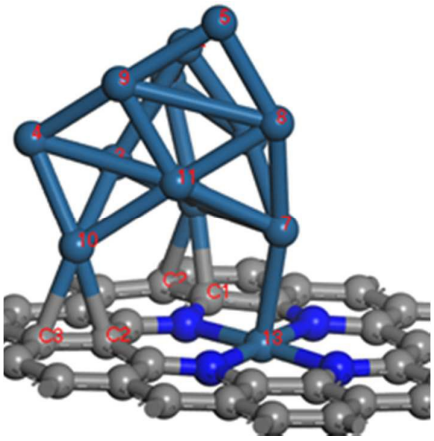

(c)

Figure 3

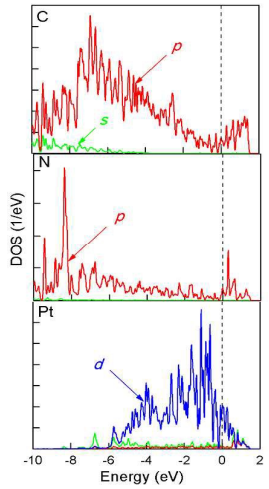

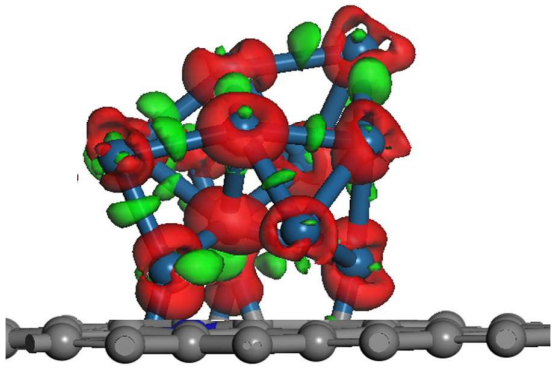

(a)

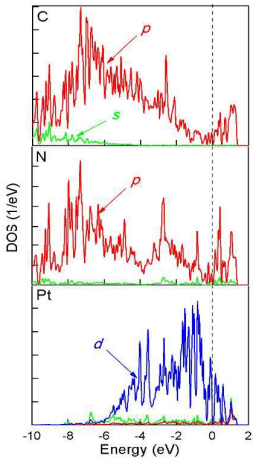

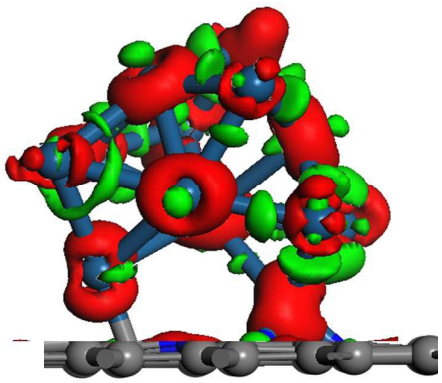

(b)

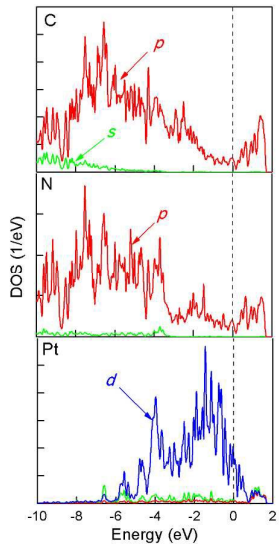

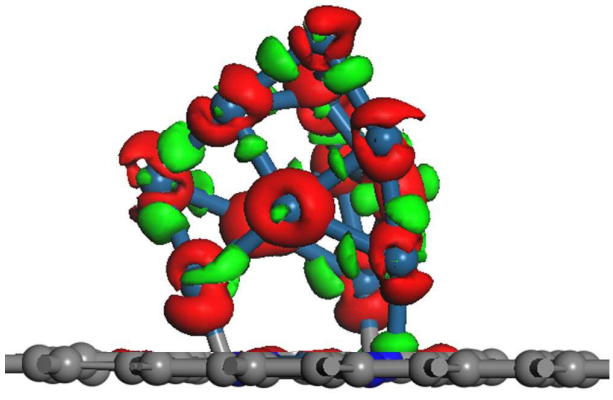

(c)

Figure 4

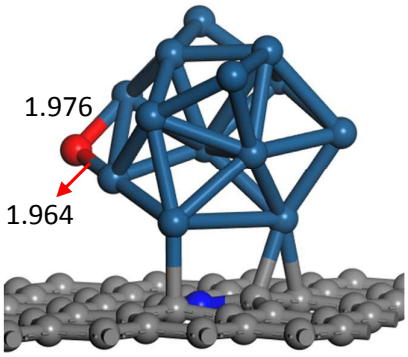

(a) E_{ads} = –1.762 eV

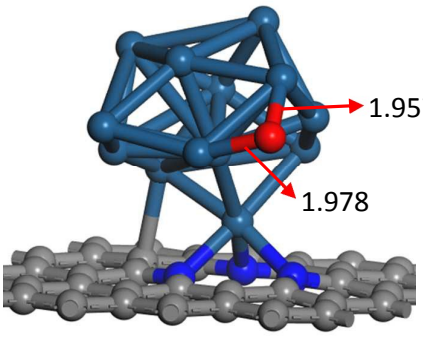

(b) E_{ads} = –1.723 eV

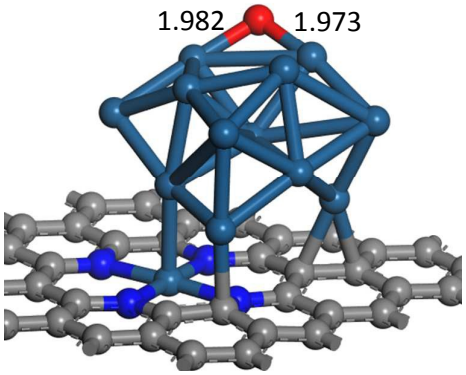

(c) E_{ads} = –1.507 eV